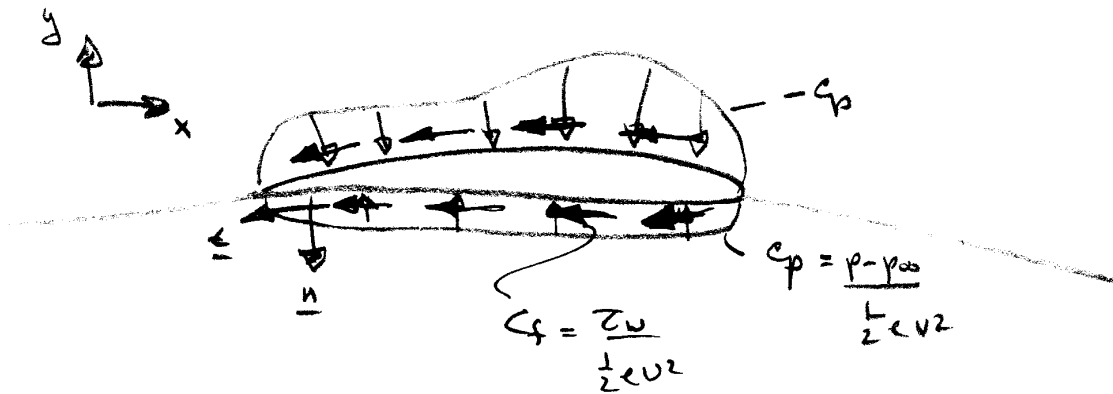


Chapter 9 Flow over Immersed Bodies

Basic Considerations

Recall separation of drag components into form and skin-friction



$$C_D = \frac{1}{\frac{1}{2} \rho V^2 A} \left\{ \underbrace{\int_S (p - p_\infty) \underline{n} \cdot \hat{i} dA}_{C_{Dp}} + \underbrace{\int_S \tau_w \underline{t} \cdot \hat{i} dA}_{C_f} \right\}$$

$$C_L = \frac{1}{\frac{1}{2} \rho V^2 A} \left\{ \int_S (p - p_\infty) \underline{n} \cdot \hat{j} dA \right\}$$

$$\frac{t}{c} \ll 1 \quad C_f \gg C_{Dp} \quad \text{streamlined body}$$

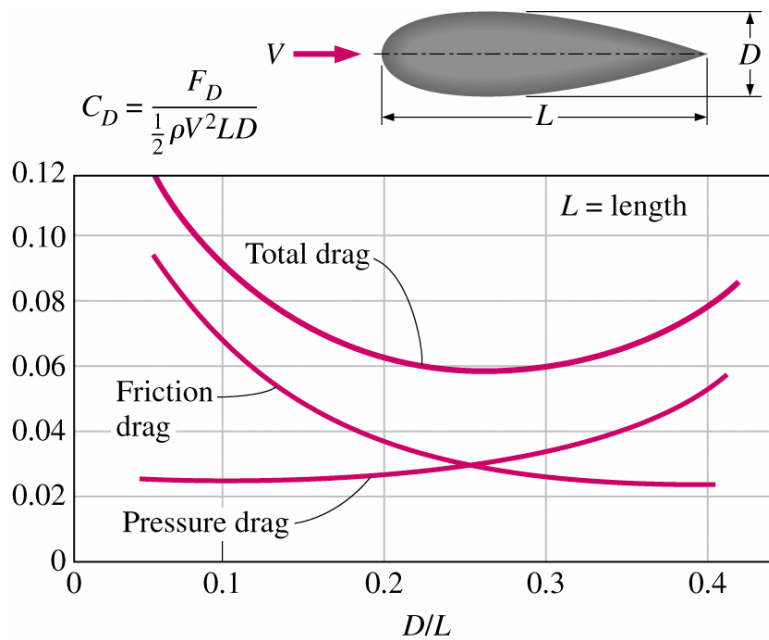
$$\frac{t}{c} \sim 1 \quad C_{Dp} \gg C_f \quad \text{bluff body}$$

Streamlining: One way to reduce the drag

Make a body streamlined:

- reduce the flow separation → reduce the pressure drag
- increase the surface area → increase the friction drag

→ **Trade-off relationship** between pressure drag and friction drag



Trade-off relationship between pressure drag and friction drag

Benefit of streamlining: reducing vibration and noise

Qualitative Description of the Boundary Layer

Recall our previous description of the flow-field regions for high Re flow about slender bodies

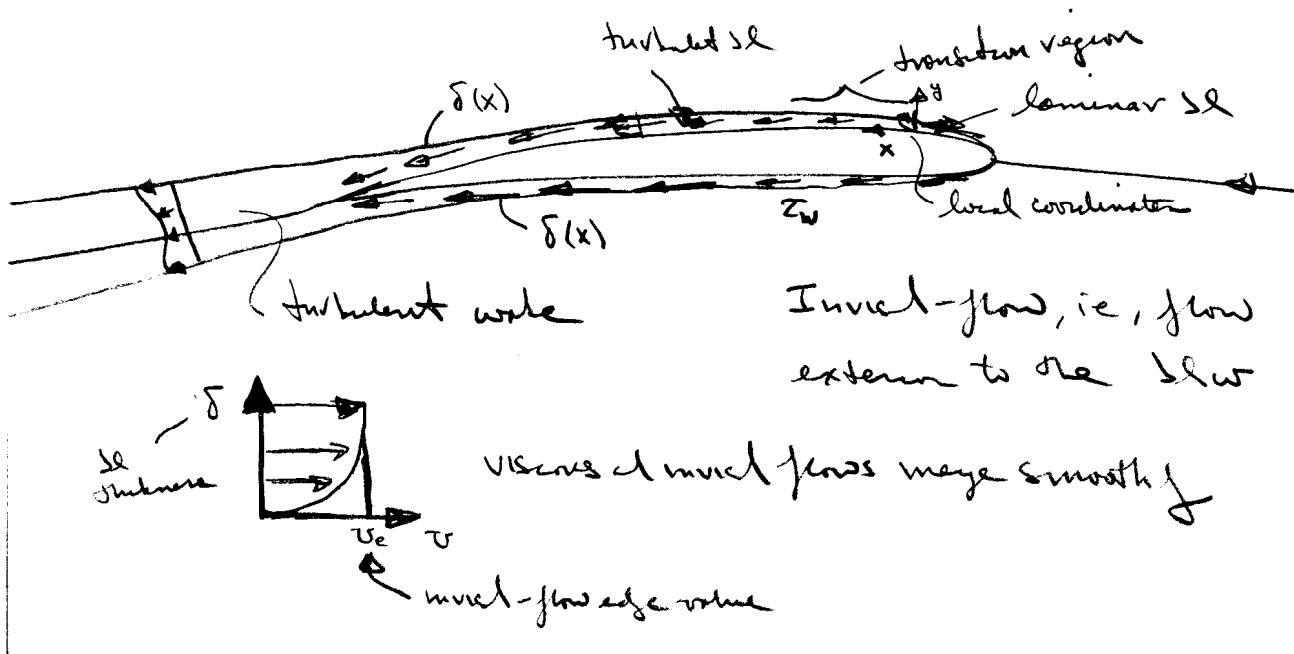
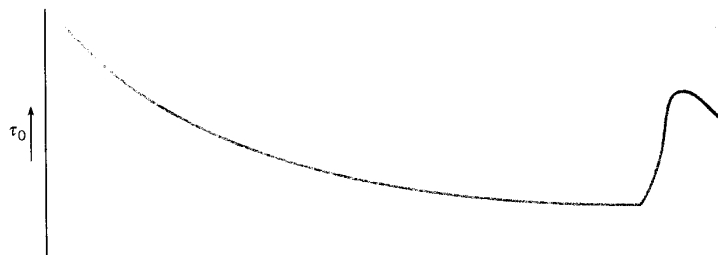
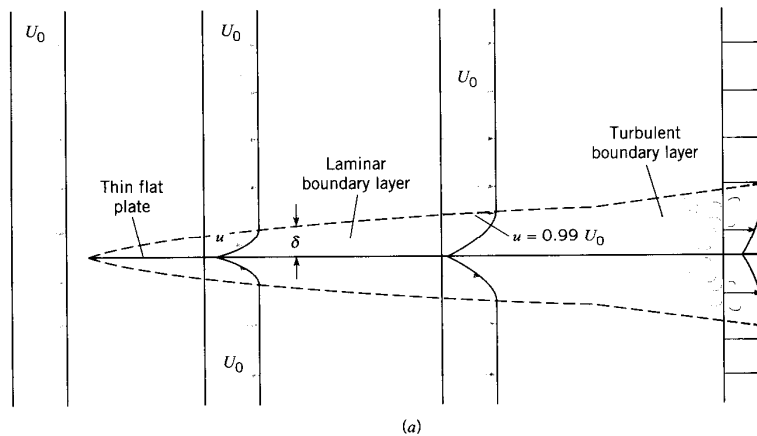


FIGURE 9.4
 Development of boundary layer and distribution of shear stress along a thin, flat plate. (a) Flow pattern in boundary layers above and below the plate. (b) Shear-stress distribution on either side of the plate.



$\tau_w = \text{shear stress}$

$\tau_w \propto \text{rate of strain (velocity gradient)}$

$$= \mu \left. \frac{\partial u}{\partial y} \right|_{y=0}$$

large near the surface where
fluid undergoes large changes to
satisfy the no-slip condition

Boundary layer theory is a simplified form of the complete NS equations and provides τ_w as well as a means of estimating C_{form} . Formally, boundary-layer theory represents the asymptotic form of the Navier-Stokes equations for high Re flow about slender bodies. As mentioned before, the NS equations are 2nd order nonlinear PDE and their solutions represent a formidable challenge. Thus, simplified forms have proven to be very useful.

Near the turn of the century (1904), Prandtl put forth boundary-layer theory, which resolved D'Alembert's paradox. As mentioned previously, boundary-layer theory represents the asymptotic form of the NS equations for high Re flow about slender bodies. The latter requirement is necessary since the theory is restricted to unseparated flow. In fact, the boundary-layer equations are singular at

separation, and thus, provide no information at or beyond separation. However, the requirements of the theory are met in many practical situations and the theory has many times over proven to be invaluable to modern engineering.

The assumptions of the theory are as follows:

Variable	order of magnitude		
u	U	$O(1)$	$\varepsilon = \delta/L$
v	$\delta \ll L$	$O(\varepsilon)$	
$\frac{\partial}{\partial x}$	L	$O(1)$	
$\frac{\partial}{\partial y}$	$1/\delta$	$O(\varepsilon^{-1})$	
ν	δ^2	ε^2	

The theory assumes that viscous effects are confined to a thin layer close to the surface within which there is a dominant flow direction (x) such that $u \sim U$ and $v \ll u$. However, gradients across δ are very large in order to satisfy the no slip condition.

Next, we apply the above order of magnitude estimates to the NS equations.

$$\left. \begin{aligned}
 u \frac{\partial u}{\partial x} + v \frac{\partial u}{\partial y} &= -\frac{\partial p}{\partial x} + \mu \left(\frac{\partial^2 u}{\partial x^2} + \frac{\partial^2 u}{\partial y^2} \right) \\
 1 \quad 1 \quad \varepsilon \quad \varepsilon^{-1} & \quad \quad \varepsilon^2 \quad 1 \quad \varepsilon^{-2} \\
 \\
 u \frac{\partial v}{\partial x} + v \frac{\partial v}{\partial y} &= -\frac{\partial p}{\partial y} + \mu \left(\frac{\partial^2 v}{\partial x^2} + \frac{\partial^2 v}{\partial y^2} \right) \\
 1 \quad \varepsilon \quad \varepsilon \quad 1 & \quad \quad \varepsilon^2 \quad 1 \quad \varepsilon^{-1} \\
 \\
 \frac{\partial u}{\partial x} + \frac{\partial v}{\partial y} &= 0 \\
 1 \quad 1 &
 \end{aligned} \right\} \text{elliptic}$$

Retaining terms of $O(1)$ only results in the celebrated boundary-layer equations

$$\left. \begin{aligned}
 u \frac{\partial u}{\partial x} + v \frac{\partial u}{\partial y} &= -\frac{\partial p}{\partial x} + \mu \frac{\partial^2 u}{\partial y^2} \\
 \\
 \frac{\partial p}{\partial y} &= 0 \\
 \\
 \frac{\partial u}{\partial x} + \frac{\partial v}{\partial y} &= 0
 \end{aligned} \right\} \text{parabolic}$$

Some important aspects of the boundary-layer equations:

- 1) the y-momentum equation reduces to

$$\frac{\partial p}{\partial y} = 0$$

i.e., $p = p_e = \text{constant across the boundary layer}$

from the Bernoulli equation:

$$p_e + \frac{1}{2}\rho U_e^2 = \text{constant}$$

i.e., $\frac{\partial p_e}{\partial x} = -\rho U_e \frac{\partial U_e}{\partial x}$

edge value, i.e.,
 inviscid flow value!

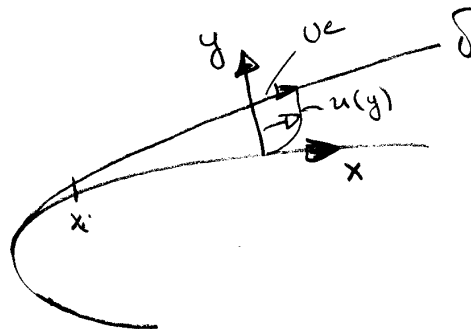
Thus, the boundary-layer equations are solved subject to a specified inviscid pressure distribution

- 2) continuity equation is unaffected
- 3) Although NS equations are fully elliptic, the boundary-layer equations are parabolic and can be solved using marching techniques

4) Boundary conditions

$$u = v = 0 \quad y = 0$$

$$u = U_e \quad y = \delta$$



+ appropriate initial conditions @ x_i

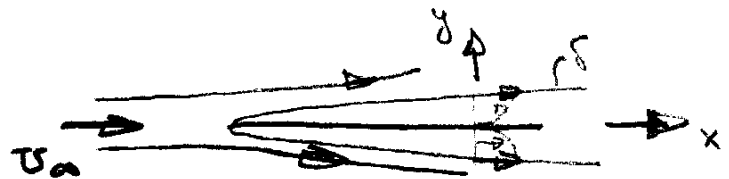
There are quite a few analytic solutions to the boundary-layer equations. Also numerical techniques are available for arbitrary geometries, including both two- and three-dimensional flows. Here, as an example, we consider the

simple, but extremely important case of the boundary layer development over a flat plate.

Quantitative Relations for the Laminar Boundary Layer

Laminar boundary-layer over a flat plate: Blasius solution (1908) student of Prandtl \rightarrow

$$\frac{\partial u}{\partial x} + \frac{\partial v}{\partial y} = 0$$



Note: $\frac{\partial p}{\partial x} = 0$
 for a flat plate

$$u \frac{\partial u}{\partial x} + v \frac{\partial u}{\partial y} = \nu \frac{\partial^2 u}{\partial y^2}$$

$$u = v = 0 \quad @ \quad y = 0$$

$$u = U_\infty \quad @ \quad y = \delta$$

We now introduce a dimensionless transverse coordinate and a stream function, i.e.,

$$\eta = y \sqrt{\frac{U_\infty}{\nu x}} \propto \frac{y}{\delta}$$

$$\psi = \sqrt{\nu x U_\infty} f(\eta)$$

$$u = \frac{\partial \psi}{\partial y} = \frac{\partial \psi}{\partial \eta} \frac{\partial \eta}{\partial y} = U_\infty f'(\eta)$$

$$f' = u / U_\infty$$

$$v = -\frac{\partial \psi}{\partial x} = \frac{1}{2} \sqrt{\frac{v U_\infty}{x}} (\eta f' - f)$$

substitution into the boundary-layer equations yields

$$ff'' + 2f''' = 0 \quad \text{Blasius Equation}$$

$$f = f' = 0 \quad @ \quad \eta = 0 \quad \quad f' = 1 \quad @ \quad \eta = 1$$

The Blasius equation is a 3rd order ODE which can be solved by standard methods (Runge-Kutta). Also, series solutions are possible. Interestingly, although simple in appearance no analytic solution has yet been found. Finally, it should be recognized that the Blasius solution is a similarity solution, i.e., the non-dimensional velocity profile f' vs. η is independent of x . That is, by suitably scaling all the velocity profiles have neatly collapsed onto a single curve.

Now, lets consider the characteristics of the Blasius solution:

$$\frac{u}{U_\infty} \text{ vs. } y$$

$$\frac{v}{U_\infty} \sqrt{\frac{U_\infty}{\nu}} \text{ vs. } y$$

$$\delta = \frac{5x}{\sqrt{Re}}$$

value of y where $u/U_\infty = .99$

$$Re_x = \frac{U_\infty x}{\nu}$$

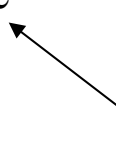


FIGURE 9.5
 Velocity distribution in
 laminar boundary layer.
 [After Blasius (3)].

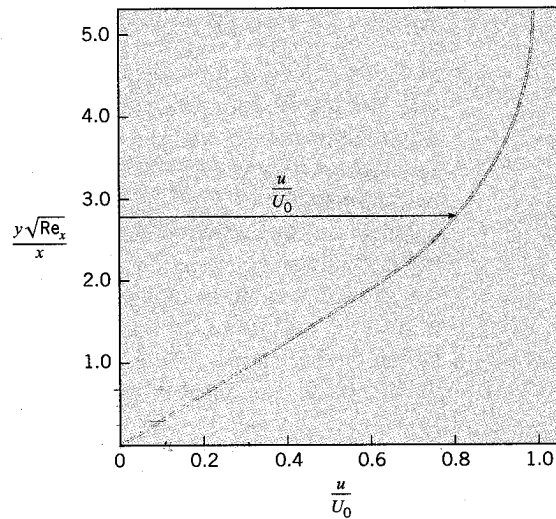


TABLE 9.1 RESULTS— δ AND τ_0 FOR DIFFERENT VALUES OF x

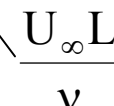
	$x = 0.1$ ft	$x = 1.0$ ft	$x = 2$ ft	$x = 4$ ft	$x = 6$ ft
$x^{1/2}$	0.316	1.00	1.414	2.00	2.45
τ_0 , psf	0.552	0.174	0.123	0.087	0.071
δ , ft	0.005	0.016	0.022	0.031	0.039
δ , in.	0.060	0.189	0.270	0.380	0.466

$$\tau_w = \frac{\mu U_\infty f''(0)}{\sqrt{2\nu x / U_\infty}}$$

i.e.,
$$c_f = \frac{2\tau_w}{\rho U_\infty^2} = \frac{0.664}{\sqrt{Re_x}} = \frac{\theta}{x} \leftarrow \text{see below}$$


$$C_f = \frac{1}{L} \int_0^L c_f dx = 2c_f(L)$$

$$= \frac{1.328}{\sqrt{\text{Re}_L}}$$



 $\frac{U_\infty L}{\nu}$

Other:

$$\delta^* = \int_0^\delta \left(1 - \frac{u}{U_\infty}\right) dy = 1.7208 \frac{x}{\sqrt{\text{Re}_x}} \quad \text{displacement thickness}$$


 measure of displacement of inviscid flow to due boundary layer

$$\theta = \int_0^\delta \left(1 - \frac{u}{U_\infty}\right) \frac{u}{U_\infty} dy = 0.664 \frac{x}{\sqrt{\text{Re}_x}} \quad \text{momentum thickness}$$


 measure of loss of momentum due to boundary layer

$$H = \text{shape parameter} = \frac{\delta^*}{\theta} = 2.5916$$

Quantitative Relations for the Turbulent Boundary Layer

2-D Boundary-layer Form of RANS equations

$$\frac{\partial u}{\partial x} + \frac{\partial v}{\partial y} = 0$$

$$u \frac{\partial u}{\partial x} + v \frac{\partial u}{\partial y} = -\frac{\partial}{\partial x} \left(\frac{p_e}{\rho} \right) + \nu \frac{\partial^2 u}{\partial y^2} - \underbrace{\frac{\partial}{\partial y} (\overline{u'v'})}_{\text{requires modeling}}$$

Momentum Integral Analysis

Background: History and Modern Approach: FD

To obtain general momentum integral relation which is valid for both laminar and turbulent flow

∞ For flat plate or δ for general case

$$\int_{y=0}^{\infty} (\text{momentum equation} + (u - v) \text{ continuity}) dy$$

$$\frac{\tau_w}{\rho U^2} = \frac{1}{2} c_f = \frac{d\theta}{dx} + (2 + H) \frac{\theta}{U} \frac{dU}{dx} \quad -\frac{dp}{dx} = \rho U \frac{dU}{dx}$$

flat plate equation $\frac{dU}{dx} = 0$

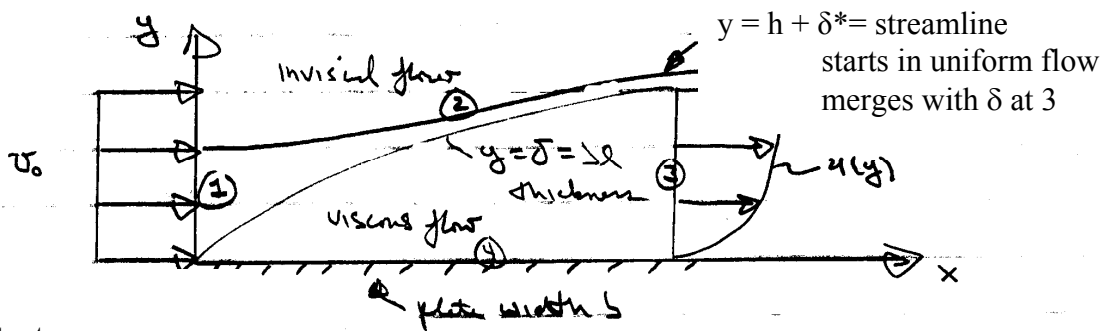
$$\theta = \int_0^{\delta} \frac{u}{U} \left(1 - \frac{u}{U} \right) dy \quad \text{momentum thickness}$$

$$H = \frac{\delta^*}{\theta} \quad \text{shape parameter}$$

$$\delta^* = \int_0^{\delta} \left(1 - \frac{u}{U} \right) dy \quad \text{displacement thickness}$$

Can also be derived by CV analysis as shown next for flat plate boundary layer.

Momentum Equation Applied to the Boundary Layer



Steady
 $\rho = \text{constant}$
 neglect g
 $v \ll u = u_0 \Rightarrow p = \text{constant}$
 i.e., $-\nabla p = 0$

CV = 1, 2, 3, 4

$$-D = \text{drag} = b \int_0^x \tau_w dx \quad \text{pressure force} = 0 \text{ for } v \ll U_0$$

force on CV wall shear stress $u \sim U_0$

$$\begin{aligned} \sum F_x &= -D = \rho \int_1 u(\underline{V} \cdot d\underline{A}) + \rho \int_3 u(\underline{V} \cdot d\underline{A}) \\ &= \rho(-U_0^2 bh) + \rho b \int_3 u^2 dy \end{aligned}$$

$$D(x) = \rho U_0^2 bh - \rho b \int_0^\delta u^2 dy$$

next eliminate h using continuity

$$0 = \rho \int_1 \underline{V} \cdot \underline{dA} + \rho \int_3 \underline{V} \cdot \underline{dA}$$

$$\rho U_o b h = \rho b \int_0^{\delta} u dy \leftarrow \text{depends on } u(y)$$

$$U_o h = \int_0^{\delta} u dy$$

$$\begin{aligned} D(x) &= \rho b U_o \int_0^{\delta} u dy - \rho b \int_0^{\delta} u^2 dy \\ &= \rho b \int_0^{\delta} u (U_o - u) dy \end{aligned}$$

$$C_D = \frac{D}{\frac{1}{2} \rho U_o^2 b L} = \frac{2}{L} \int_0^{\delta} \frac{u}{U_o} \left(1 - \frac{u}{U_o} \right) dy$$

$\theta = \text{momentum thickness}$

$$C_D = \frac{2\theta}{L}$$

$$C_D = \frac{D}{\frac{1}{2} \rho U_o^2 A} = \frac{b \int_0^x \tau_w dx}{\frac{1}{2} \rho U_o^2 b L} = \frac{2\theta}{L}$$

$$\int_0^x \frac{\tau_w}{\frac{1}{2}\rho U_o^2}(x)dx = 2\theta(x)$$

$$\frac{1}{2} \left(\frac{\tau_w}{\frac{1}{2}\rho U_o^2} \right) = \frac{d\theta}{dx}$$

$$\frac{c_f}{2} = \frac{d\theta}{dx} \quad c_f = \text{local skin friction coefficient}$$

momentum integral relation for flat plate boundary layer

$$\theta = \int_0^{\delta} \frac{u}{u_o} \left(1 - \frac{u}{u_o} \right) dy$$

Approximate solution for a laminar boundary-layer

Assume cubic polynomial for u(y)

$$\frac{u}{U_\infty} = A + By + Cy^2 + Dy^3$$

$$\left. \begin{array}{l} u = \frac{\partial^2 u}{\partial y^2} = 0 \quad y = 0 \\ u = U_\infty; \frac{\partial u}{\partial y} = 0 \quad y = \delta \end{array} \right\} \begin{array}{l} A = 0 \quad B = \frac{3}{2}\delta \\ C = 0 \quad D = -\frac{1}{2}\delta^3 \end{array}$$

$$\text{i.e., } \frac{u}{U} = \frac{3y}{2\delta} + \frac{1}{2} \left(\frac{y}{\delta} \right)^3 \qquad u_y = U \left(\frac{3}{2\delta} + \frac{3y^2}{2\delta^3} \right) \Big|_{y=0} = \frac{U3}{2\delta}$$

$\frac{\tau_w}{\rho U^2} = \frac{1}{2} c_f = \frac{d\theta}{dx}$	momentum integral equation for $\frac{dp}{dx} = 0$
--	--

$$\frac{1}{\rho U^2} \left[\underbrace{\mu U \frac{3}{2\delta}}_{\tau_w} \right] = .139 \frac{d\delta}{dx}$$

$$\theta = \int_0^{\delta} \frac{u}{U} \left(1 - \frac{u}{U} \right) dy$$

$$\tau_w = \mu \frac{du}{dy}$$

Compare with
 Exact Blasius

i.e.,	$\delta = \frac{4.65x}{\sqrt{Re_x}}$	$\frac{5x}{\sqrt{Re_x}} \quad 7\% \downarrow$
-------	--------------------------------------	---

	$\tau_w = \frac{.323\rho V^2}{\sqrt{Re_x}}$	$\frac{.332\rho U^2}{\sqrt{Re_x}} \quad 3\% \downarrow$
--	---	---

	$c_f = \frac{.646}{\sqrt{Re_x}}$	$\frac{.664}{\sqrt{Re_x}}$
--	----------------------------------	----------------------------

	$C_f = \frac{1.29}{\sqrt{Re_L}}$	$\frac{1.33}{\sqrt{Re_L}}$
--	----------------------------------	----------------------------

$$C_f = \frac{1}{\frac{1}{2}\rho U^2 b L} \int_0^L \tau_w(x) dx$$

total skin-friction drag coefficient

Approximate solution Turbulent Boundary-Layer

$Re_t \sim 3 \times 10^6$ for a flat plate boundary layer
 $Re_{crit} \sim 500,000$

$$\frac{c_f}{2} = \frac{d\theta}{dx}$$

as was done for the approximate laminar flat plate boundary-layer analysis, solve by expressing $c_f = c_f(\delta)$ and $\theta = \theta(\delta)$ and integrate, i.e.

assume log-law valid across entire turbulent boundary-layer

$$\frac{u}{u^*} = \frac{1}{\kappa} \ln \frac{yu^*}{\nu} + B$$

neglect laminar sub layer
and velocity defect region

at $y = \delta, u = U$

$$\frac{U}{u^*} = \frac{1}{\kappa} \ln \frac{\delta u^*}{\nu} + B$$

$$\left. \begin{aligned} \text{or } \left(\frac{2}{c_f}\right)^{1/2} &= 2.44 \ln \left[\text{Re}_\delta \left(\frac{c_f}{2}\right)^{1/2} \right] + 5 \\ c_f &\cong .02 \text{Re}_\delta^{-1/6} \text{ power-law fit} \end{aligned} \right\} c_f(\delta)$$

Next, evaluate

$$\frac{d\theta}{dx} = \frac{d}{dx} \int_0^\delta \frac{u}{U} \left(1 - \frac{u}{U}\right) dy$$

can use log-law or more simply a power law fit

$$\left. \begin{aligned} \frac{u}{U} &= \left(\frac{y}{\delta}\right)^{1/7} \\ \theta &= \frac{7}{72} \delta = \theta(\delta) \end{aligned} \right\} \begin{aligned} &\text{Note: can not be} \\ &\text{used to obtain } c_f(\delta) \\ &\text{since } \tau_w \rightarrow \infty \end{aligned}$$

$$\Rightarrow \tau_w = c_f \frac{1}{2} \rho U^2 = \rho U^2 \frac{d\theta}{dx} = \frac{7}{72} \rho U^2 \frac{d\delta}{dx}$$

$$\text{Re}_\delta^{-1/6} = 9.72 \frac{d\delta}{dx}$$

$$\text{or } \frac{\delta}{x} = .16 \text{Re}_x^{-1/7} \quad \begin{array}{l} \text{i.e., much faster} \\ \text{growth rate than} \\ \text{laminar} \\ \text{boundary layer} \end{array}$$

$$\delta \propto x^{6/7} \quad \text{almost linear}$$

$$c_f = \frac{.027}{\text{Re}_x^{1/7}}$$

$$C_f = \frac{.031}{\text{Re}_L^{1/7}} = \frac{7}{6} C_f(L)$$

Alternate forms given in text depending on experimental information and power-law fit used, etc. (i.e., dependent on Re range.)

Some additional relations given in texts for larger Re are as follows:

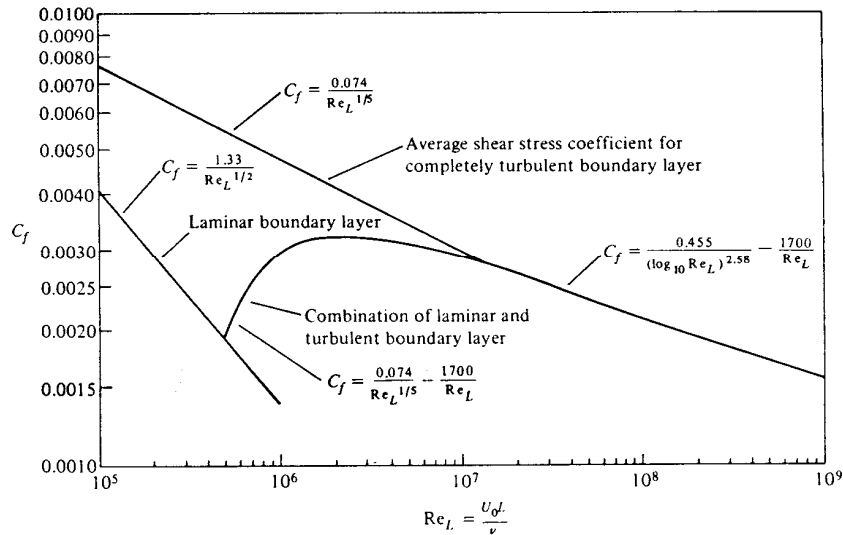
Total shear-stress coefficient

$$C_f = \frac{.455}{(\log_{10} Re_L)^{2.58}} - \frac{1700}{Re_L} \quad Re > 10^7$$

$$\frac{\delta}{L} = c_f (.98 \log Re_L - .732)$$

Local shear-stress coefficient

$$c_f = (2 \log Re_x - .65)^{-2.3}$$



Finally, a composite formula that takes into account both the initial laminar boundary-layer (with translation at $Re_{CR} = 500,000$) and subsequent turbulent boundary layer

is $C_f = \frac{.074}{Re_L^{1/5}} - \frac{1700}{Re_L} \quad 10^5 \leq Re \leq 10^7$

Drag of 2-D Bodies

First consider a flat plate both parallel and normal to the flow

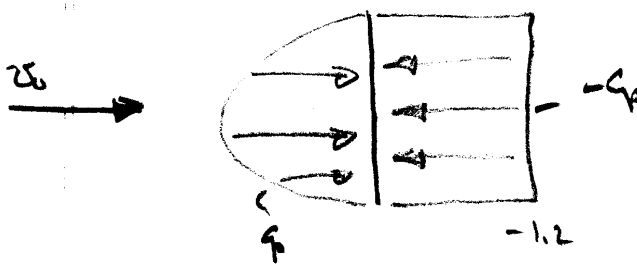


$$C_{Dp} = \frac{1}{\frac{1}{2}\rho V^2 A^s} \int (p - p_\infty) \underline{n} \cdot \underline{i} = 0$$

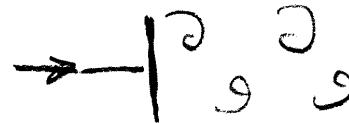
$$C_f = \frac{1}{\frac{1}{2}\rho V^2 A^s} \int \tau_w \underline{t} \cdot \underline{\hat{i}} dA$$

$$= \frac{1.33}{Re_L^{1/2}} \quad \text{laminar flow}$$

$$= \frac{.074}{Re_L^{1/5}} \quad \text{turbulent flow}$$



flow pattern



vortex wake
 typical of bluff body flow

where C_p based on experimental data

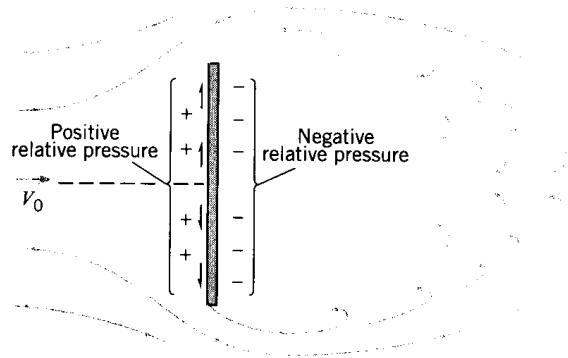
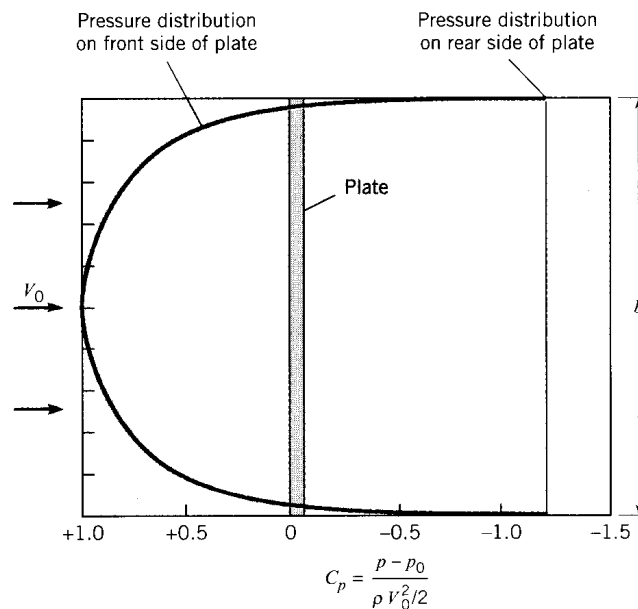


FIGURE 11.3
Flow past a flat plate.

FIGURE 11.4
Pressure distribution on a plate normal to the approach flow for $Re > 10^4$.



$$\begin{aligned}
 C_{Dp} &= \frac{1}{\frac{1}{2} \rho V^2 A^S} \int (p - p_\infty) \underline{n} \cdot \hat{i} dA \\
 &= \frac{1}{A^S} \int C_p dA \\
 &= 2 \quad \text{using numerical integration of experimental data}
 \end{aligned}$$

Potential Flow Solution: $\psi = -U_\infty \left(r - \frac{a^2}{r} \right) \sin \theta$

$$p + \frac{1}{2} \rho V^2 = p_\infty + \frac{1}{2} \rho U_\infty^2 \qquad u_r = \frac{1}{r} \frac{\partial \psi}{\partial \theta}$$

$$C_p = \frac{p - p_\infty}{\frac{1}{2} \rho U_\infty^2} = 1 - \frac{u_r^2 + u_\theta^2}{U_\infty^2} \qquad u_\theta = -\frac{\partial \psi}{\partial r}$$

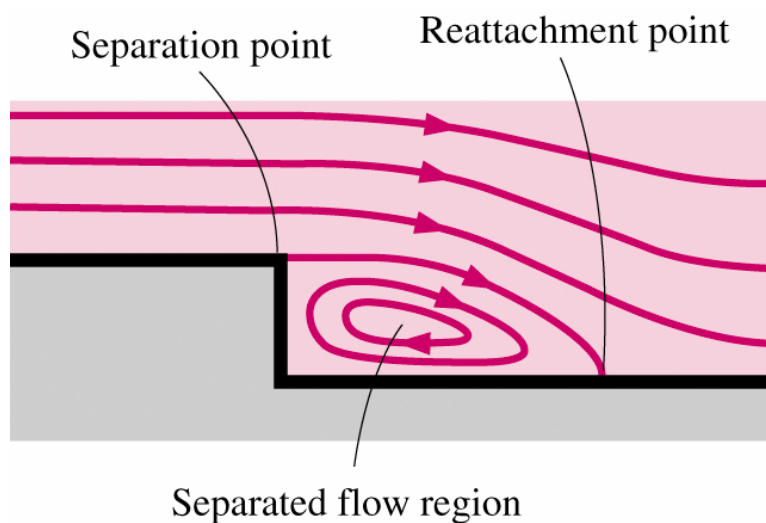
$$C_p(r = a) = 1 - 4 \sin^2 \theta \longleftarrow \text{surface pressure}$$

Flow Separation

Flow separation:

→ The fluid stream detaches itself from the surface of the body at sufficiently high velocities. Only appeared in **viscous flow!!**

Flow separation forms the region called ‘separated region’



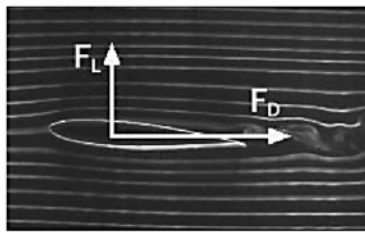
Inside the separation region:

- low-pressure, existence of recirculating/backflows
- viscous and rotational effects are the most significant!

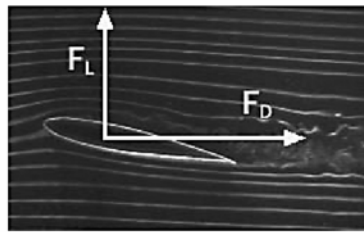
Important physics related to flow separation:

- 'Stall' for airplane (Recall the movie you saw at CFD-PreLab2!)
- Vortex shedding

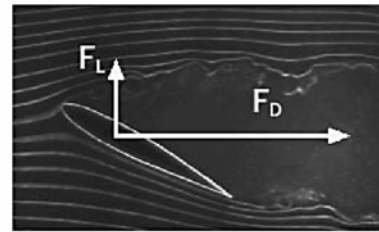
(Recall your work at CFD-Lab2, $AOA=16^\circ$! What did you see in your velocity-vector plot at the trailing edge of the air foil?)



(a) 5°



(b) 15°



(c) 30°

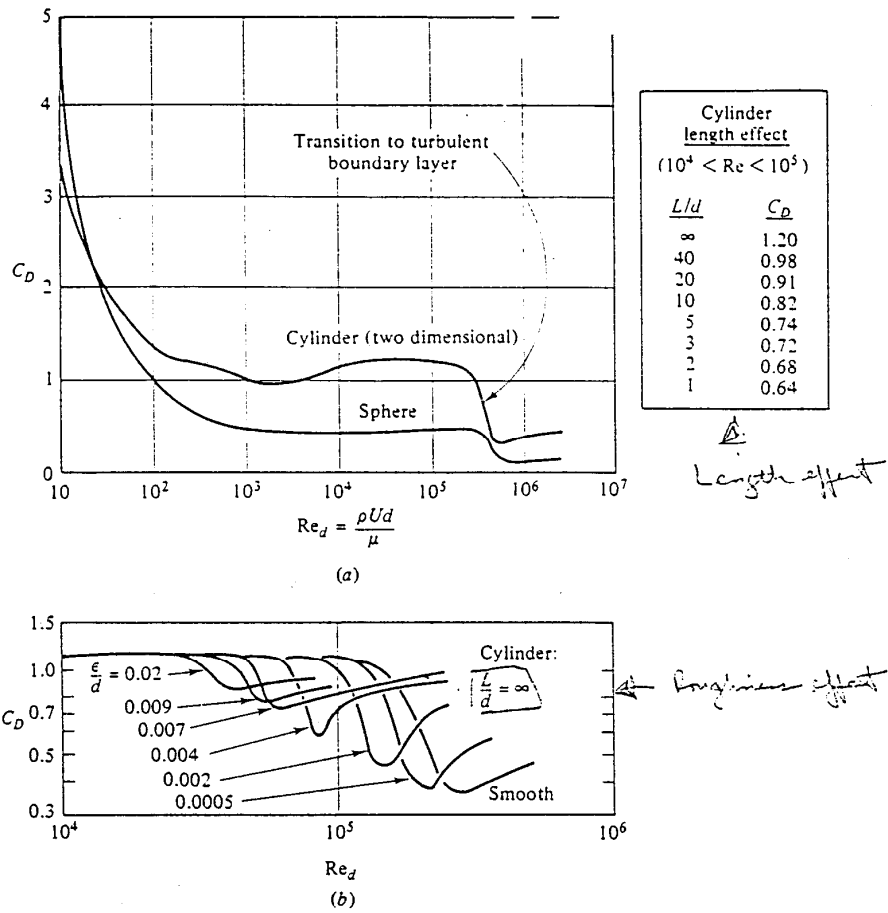


Fig. 5.3 The proof of practical dimensional analysis: drag coefficients of a cylinder and sphere: (a) drag coefficient of a smooth cylinder and sphere (data from many sources); (b) increased roughness causes earlier transition to a turbulent boundary layer.

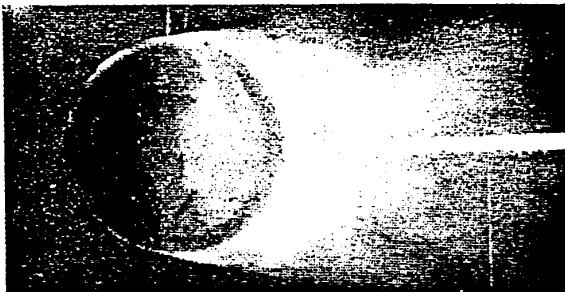


FIG. 34.—Flow round sphere below critical point. (Wieselsberger.)

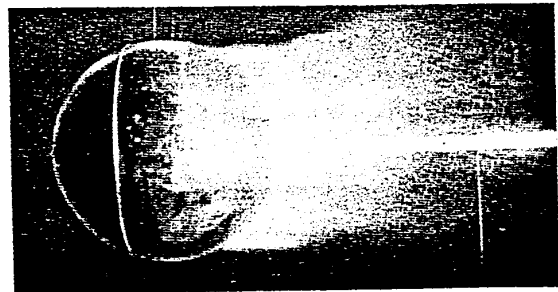


FIG. 35.—Owing to a thin wire ring round the sphere, the flow becomes of the other type with turbulent boundary layer. (Wieselsberger.)

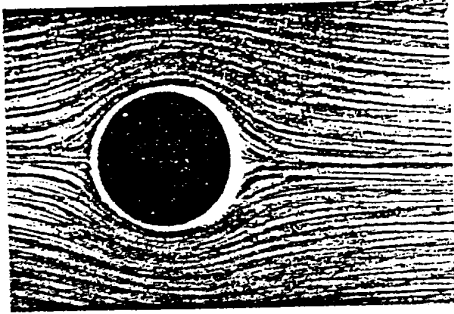


Fig. 15.5a

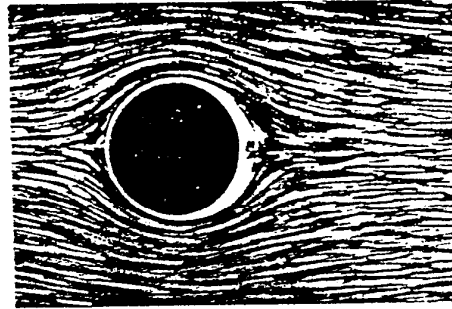


Fig. 15.5b

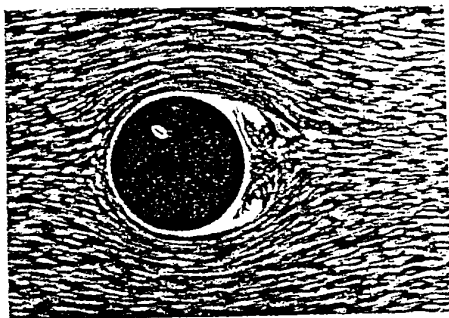


Fig. 15.5c

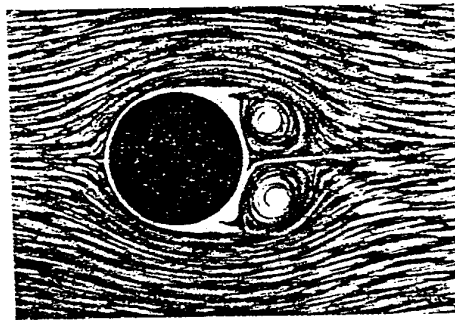


Fig. 15.5d

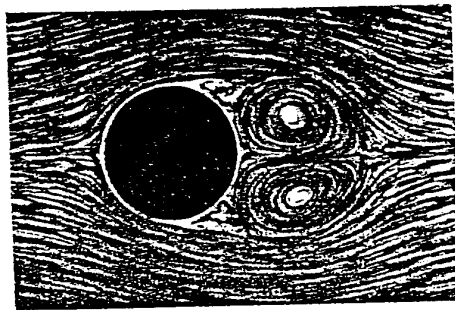


Fig. 15.5e

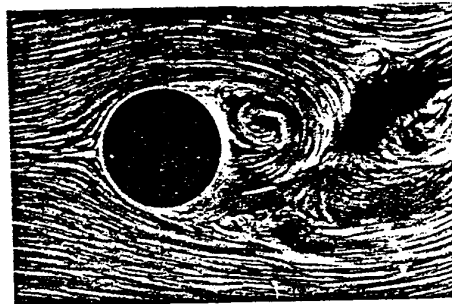
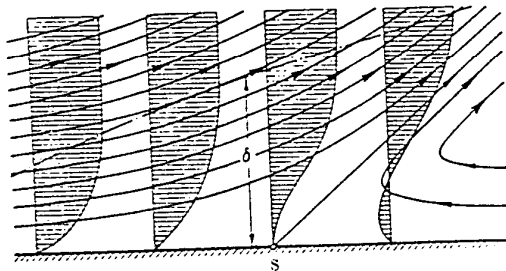


Fig. 15.5f

Fig. 15.5 a to f. Formation of vortices in flow past a circular cylinder after acceleration from rest (L. Prandtl)



S = point of separation

Fig. 2.12. Diagrammatic representation of flow in the boundary layer near a point of separation

alternate formation and shedding of vortices also creates a regular change in pressure with consequent periodicity in side thrust on the cylinder. Vortex shedding was the primary cause of failure of the Tacoma Narrows suspension bridge in the state of Washington in 1940. Another, more commonplace, effect of vortex shedding is the “singing” of wires in the wind.

If the frequency of the vortex shedding is in resonance with the natural frequency of the member that produces it, large amplitudes of vibration with consequent large stresses can develop. Experiments show that the frequency of shedding is given in terms of the Strouhal number S , and this in turn is a function of the Reynolds number. Here the Strouhal number is defined as

$$S = \frac{nd}{V_0} \quad (11-7)$$

where n is the frequency of shedding of vortices from one side of cylinder, in Hz, d is the diameter of cylinder, and V_0 is the free-stream velocity.

The relationship between the Strouhal number and the Reynolds number for vortex shedding from a circular cylinder is given in Fig. 11-10.

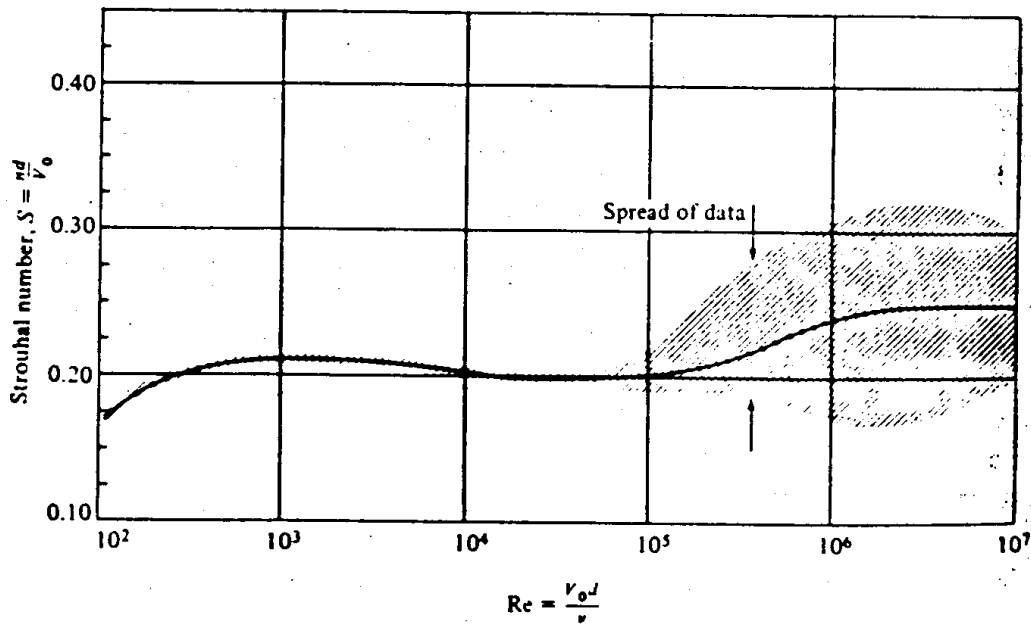


FIGURE 11-10 Strouhal number versus Reynolds number for flow past a circular cylinder. [After Jones (14) and Roshko (23)]

Other cylindrical and two-dimensional bodies also shed vortices. Consequently, the engineer should always be alert to vibration problems when designing structures that are exposed to wind or water flow.

EXAMPLE 11-2 For the cylinder and conditions of Example 11-1, at what frequency will the vortices be shed?

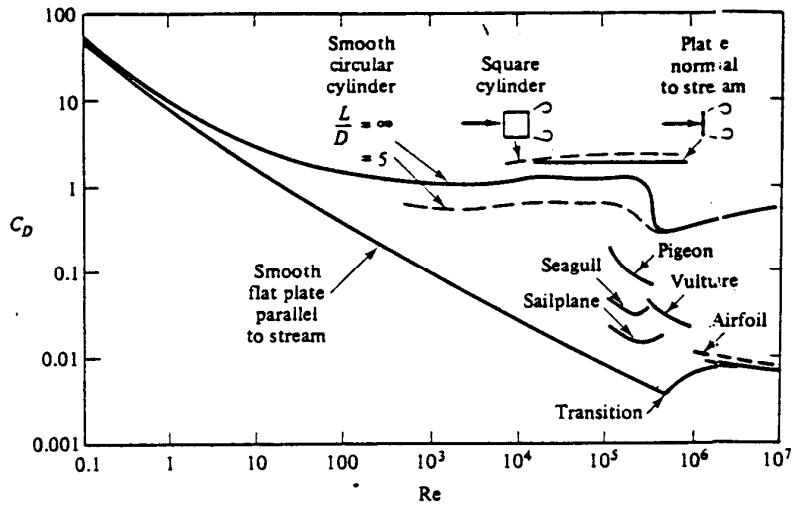


Fig. 7.16 Drag versus Reynolds number for nearly two-dimensional bodies.

Table 7.2
 DRAG OF TWO-DIMENSIONAL BODIES AT $Re = 10^5$

Shape	C_D based on frontal area	Shape	C_D based on frontal area
Plate:		Half-cylinder:	
	2.0		1.2
Square cylinder:			1.7
	2.1	Equilateral triangle:	
	1.6		1.6
Half tube:			2.0
	1.2		
	2.3		
Elliptical cylinder:			
		<u>Laminar</u>	<u>Turbulent</u>
1:1	1.2	0.3	
2:1	0.6	0.2	
4:1	0.35	0.15	
8:1	0.25	0.1	

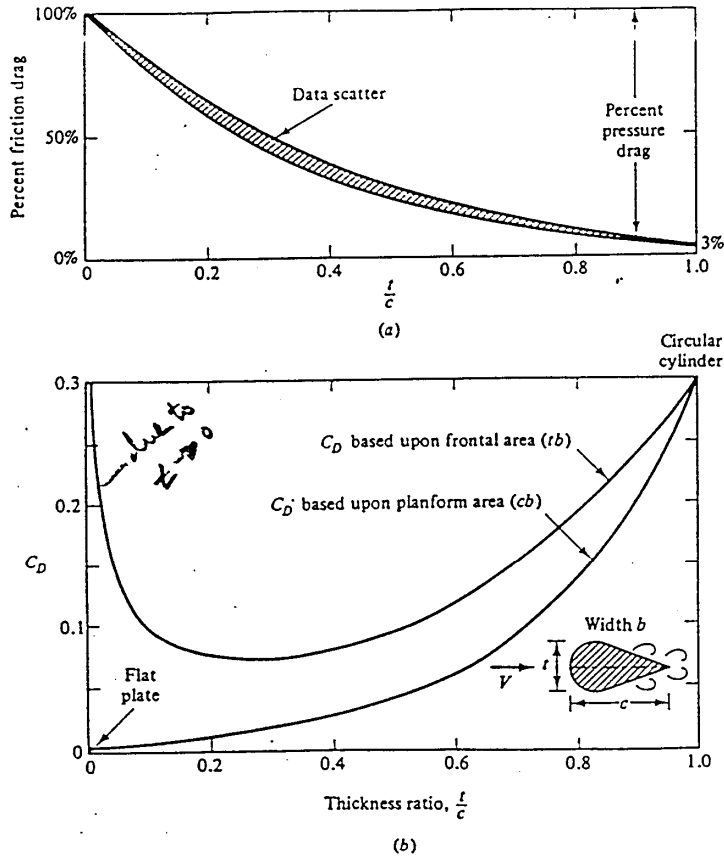


Fig. 7.12 Drag of a streamlined two-dimensional cylinder at $Re_c = 10^6$: (a) effect of thickness ratio on percentage friction drag; (b) total drag versus thickness when based upon two different areas.

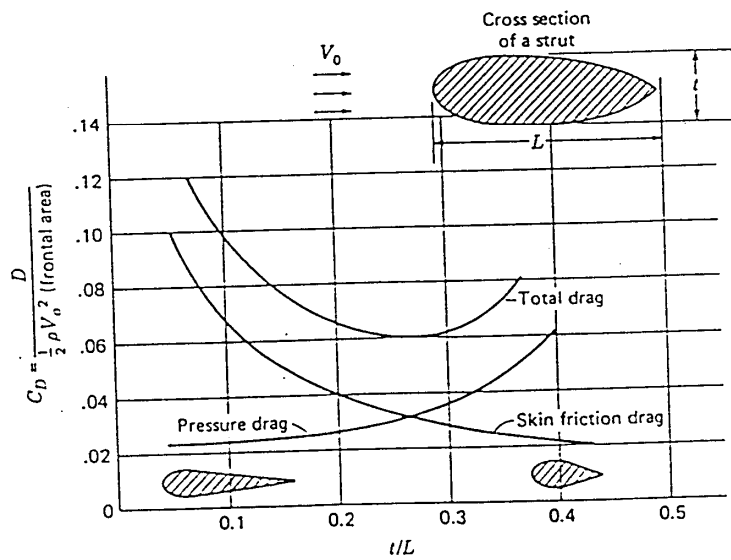


Figure 10.24 Drag coefficients for a family of struts. (S. Goldstein, "Modern Developments in Fluid Dynamics," Dover Publications, New York, 1965.)

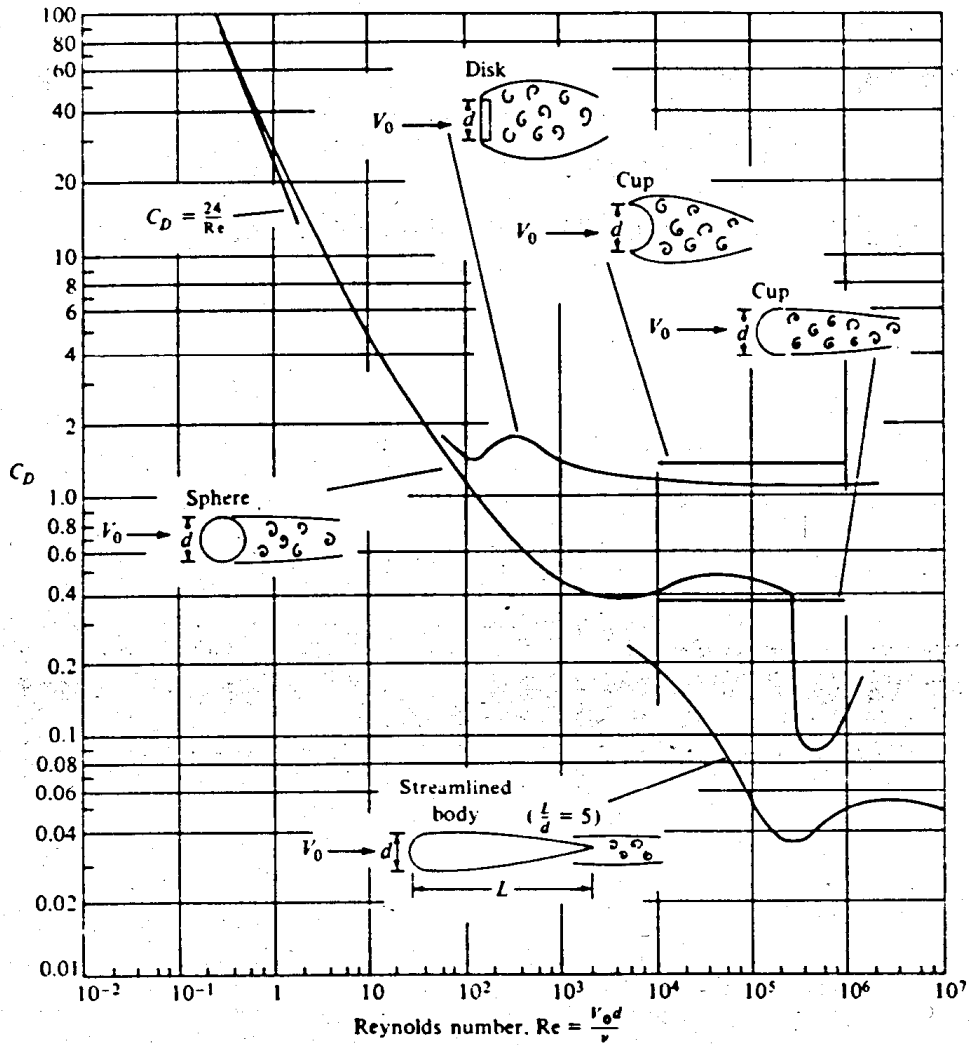
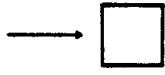
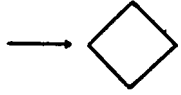
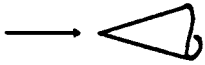
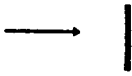
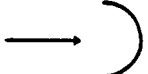
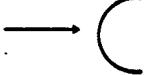
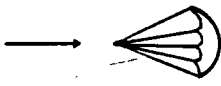
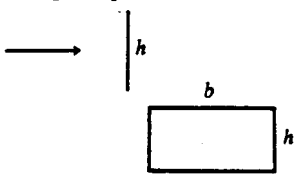
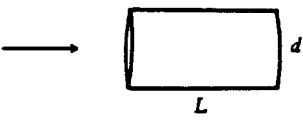
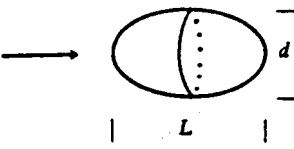


FIGURE 11-11 Coefficient of drag versus Reynolds number for axisymmetric bodies. [Data sources: Abbott (1), Breevoort (4), Freeman (9), and Rouse (24).]

Table 7.3
DRAG OF THREE-DIMENSIONAL BODIES AT $Re \approx 10^5$

Body	Ratio	C_D based on frontal area		
Cube: 		1.07		
		0.81		
60° cone: 		0.5		
Disk: 		1.17		
Cup: 		1.4		
		0.4		
Parachute (low porosity): 		1.2		
Rectangular plate: 	b/h	1	1.18	
		5	1.2	
		10	1.3	
		20	1.5	
		∞	2.0	
Flat-faced cylinder: 	L/d	0.5	1.15	
		1	0.90	
		2	0.85	
		4	0.87	
		8	0.99	
Ellipsoid: 	L/d	0.75	0.5	0.2
		1	0.47	0.2
		2	0.27	0.13
		4	0.25	0.1
		8	0.2	0.08

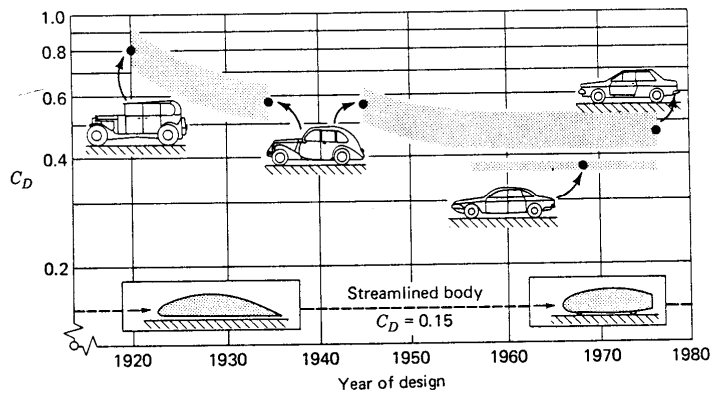


Figure 10.25 Time history of the aerodynamic drag of cars in comparison with streamlined bodies. (From Hucho, W. H., Janssen, L. J., Emmelmann, H. J., 1976, "The Optimisation of Body Details—A Method For Reducing The Aerodynamic Drag of Road Vehicles," SAE 760185.)

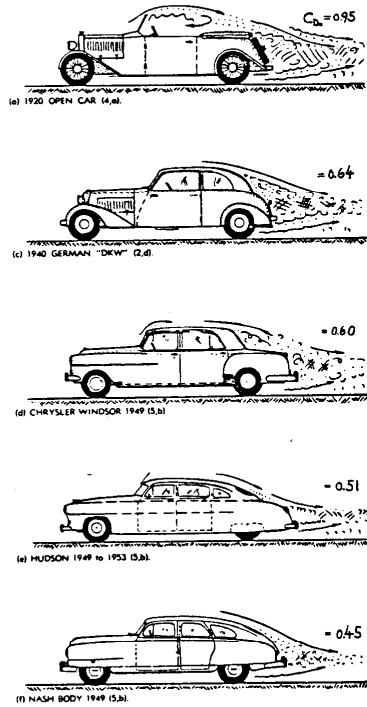


Figure 3. Drag coefficients of "standard" passenger cars, tested either in wind tunnels on geometrically similar models or by deceleration of the full-scale vehicles.

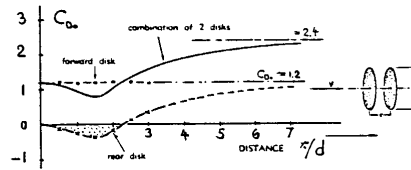


Figure 1. Interaction between two disks placed one behind the other; (reference 1,3).

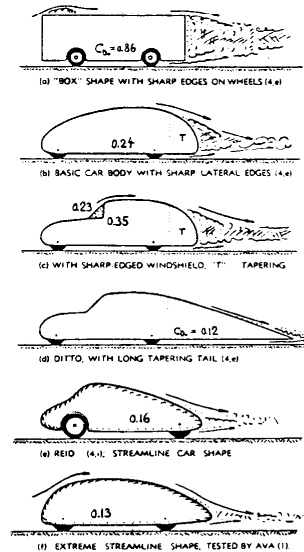


Figure 4. Drag coefficients of several smooth wind tunnel models (tested over fixed ground plate).

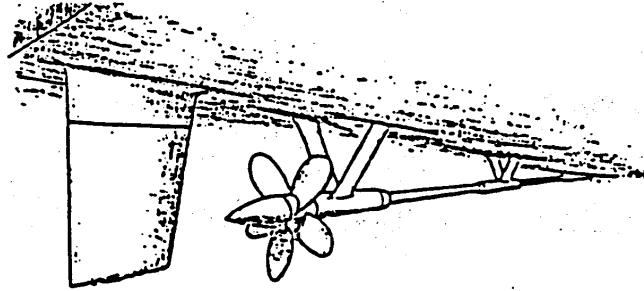


Figure 2-4. Typical naval ship stern appendages (from Kirkman, et al., 1979)

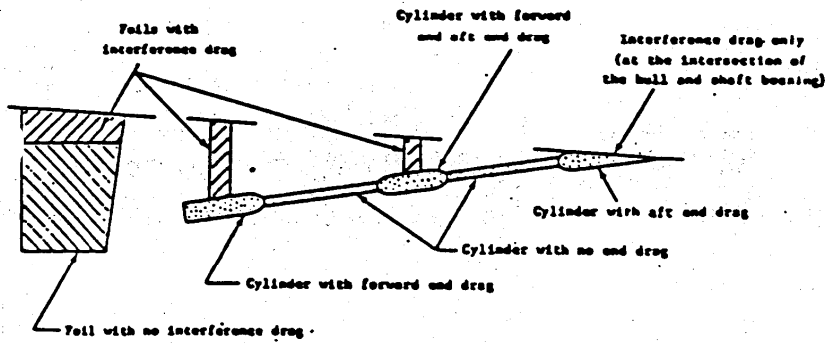


Figure 2-5. Appendage decomposition (from Kirkman, et al., 1979)

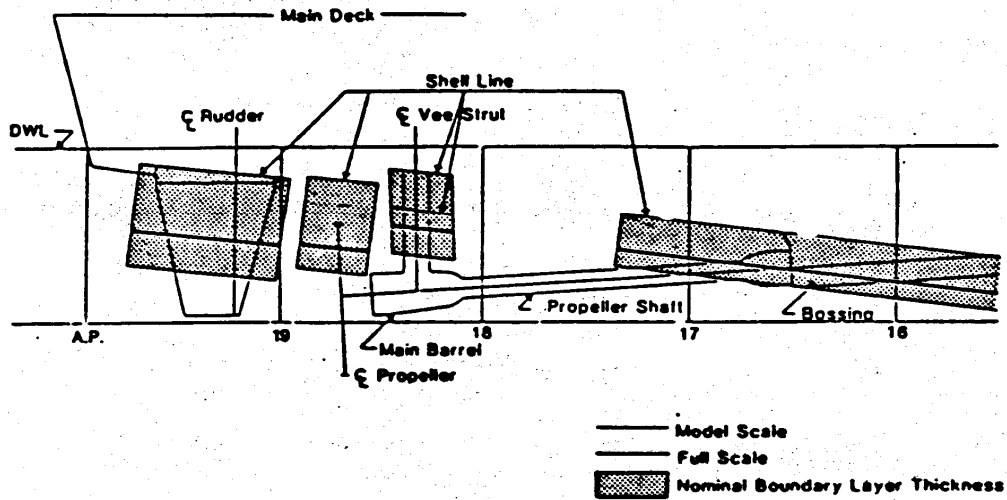
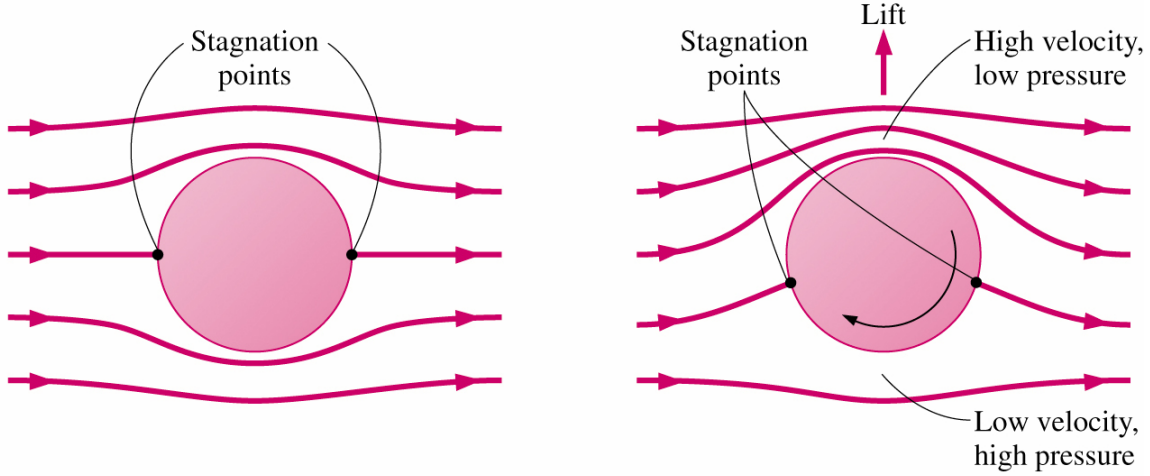


Figure 2-6. Nominal boundary layer thickness in way of the DDG 51 appendages.

Magnus effect: Lift generation by spinning

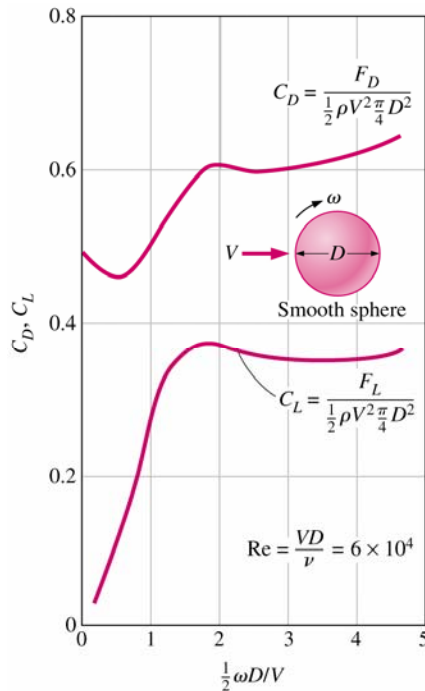
Breaking the symmetry causes the lift!



(a) Potential flow over a stationary cylinder

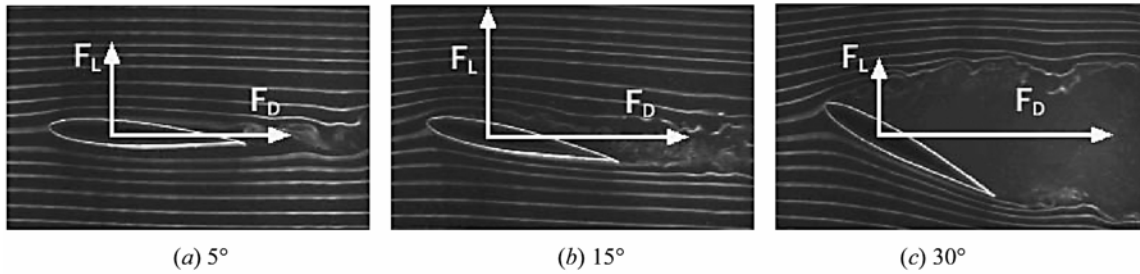
(b) Potential flow over a rotating cylinder

Effect of the rate of rotation on the lift and drag coefficients of a smooth sphere:

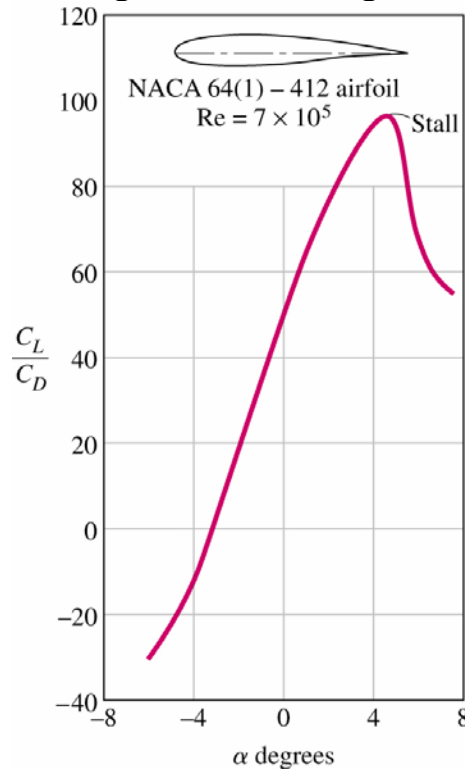


Lift acting on the airfoil

Lift force: the component of the net force (viscous+pressure) that is perpendicular to the flow direction



Variation of the lift-to-drag ratio with angle of attack:



The minimum flight velocity:

→ Total weight W of the aircraft be equal to the lift

$$W = F_L = \frac{1}{2} C_{L,max} \rho V_{min}^2 A \rightarrow V_{min} = \sqrt{\frac{2W}{\rho C_{L,max} A}}$$

Effect of Compressibility on Drag: $C_D = C_D(Re, Ma)$

$$Ma = \frac{U_\infty}{a}$$

speed of sound = rate at which infinitesimal disturbances are propagated from their source into undisturbed medium

$Ma < 1$	subsonic	≤ 0.3 flow is incompressible,
$Ma \sim 1$	transonic (=1 sonic flow)	i.e., $\rho \sim \text{constant}$
$Ma > 1$	supersonic	
$Ma \gg 1$	hypersonic	

C_D increases for $Ma \sim 1$ due to shock waves and wave drag

$Ma_{\text{critical}}(\text{sphere}) \sim .6$

$Ma_{\text{critical}}(\text{slender bodies}) \sim 1$

For $U \geq a$: upstream flow is not warned of approaching disturbance which results in the formation of shock waves across which flow properties and streamlines change discontinuously

FIGURE 11.12
 Drag characteristics of
 projectile, sphere, and
 cylinder with
 compressibility effects.
 [After Rouse (26)]

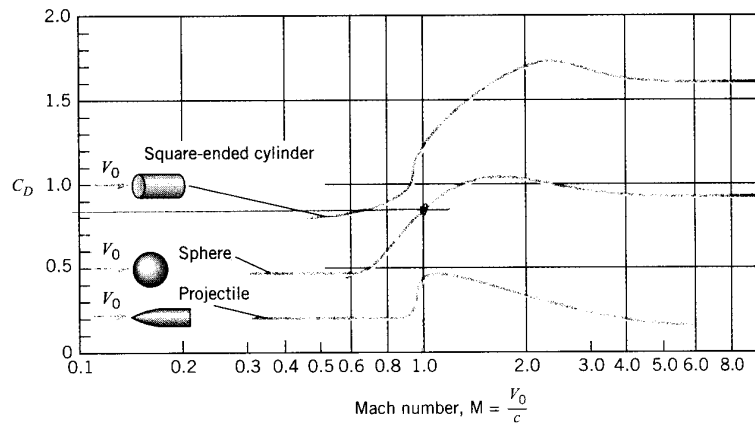


FIGURE 11.13
 Contour plot of the drag
 coefficient of the sphere
 versus Reynolds and
 Mach numbers.

